

Atom Abstraction in the Scattering of State-Selected $\text{NO}^+(X^1\Sigma^+)$ on O/Al(111)

M. Maazouz, T. L. O. Barstis*, P. L. Maazouz, and D. C. Jacobs

Department of Chemistry and Biochemistry, University of Notre Dame, Notre Dame, Indiana 46556

(Received 24 August 1999)

The reactive scattering of state-selected $\text{NO}^+(X^1\Sigma^+)$ on oxygen-covered Al(111) is explored at hyperthermal collision energies. Relative ion yields and mean translational energies of scattered NO_2^- are presented as a function of oxygen exposure and NO^+ collision energy. Above the 9 ± 1 eV threshold for reaction, NO_2^- products emerge with an average kinetic energy that depends linearly on incident NO^+ energy. The formation of NO_2^- is assigned to the direct, Eley-Rideal abstraction of an adsorbed O atom by an incident NO molecule.

PACS numbers: 79.20.Rf, 34.50.Dy, 34.70.+e

Over the last decade, hyperthermal gas-surface reactions have gained considerable attention because of their technological relevance, e.g., plasma processing in the microelectronics industry or degradation of spacecraft materials in low-earth orbit [1–3]. Ion-surface collisions span a wide range of translational energies (10^0 – 10^8 eV) and can activate unexplored surface reactions having high chemical barriers. While there has been considerable progress characterizing the dynamics of thermal reactions at surfaces, less is known about the chemical processes occurring under hyperthermal conditions. This Letter addresses the detailed mechanism of atom abstraction in the interaction of NO^+ with oxygen-covered Al(111) at 5–80 eV collision energies.

Atom abstraction is an elementary process by which an atom is transferred to or from an incident molecule as the molecule impacts a surface. Gas/surface reactions are often assigned to one of two limiting mechanisms: Langmuir-Hinshelwood (LH) or Eley-Rideal (ER) [4]. In the ER mechanism, an incident gas particle reacts directly with a surface adsorbate, whereas in the LH mechanism both reagents thermally equilibrate with the surface prior to reaction [5]. Distinguishing between ER and LH mechanisms is difficult unless one carefully probes the reaction dynamics. Three clear signatures are often associated with an ER mechanism: products emerge with a nonthermal energy distribution, the mean kinetic energy of the products correlates with the incident energy of the reactant gas [6,7], and the product angular distribution is peaked near the specular angle rather than the surface normal [8–10]. Perhaps the first definitive evidence of an ER process was obtained by Kuipers *et al.* [6] who demonstrated that $\text{N}(\text{C}_2\text{H}_4)_3\text{N}$ abstracts a proton from hydrogen-covered Pt(111) at collision energies above 1.5 eV. The translational energy of the scattered product ion was found to increase with incident energy.

Recent studies of the ER mechanism have involved exothermic reactions initiated under near-thermal conditions. Exploring the dynamics of these systems has revealed how energy is partitioned into different degrees of freedom within the products [9,11]. Hyperthermal molecular ions are relatively efficient at abstracting

atomic/molecular fragments from surface adlayers. For example, Qinyuan and Hanley established that 32 eV pyridine projectiles can abstract a proton from pyridine-covered Ag(111) [12]. Cooks and co-workers demonstrated that polyatomic projectile ions, such as pyrazine and pyrene, can abstract H, F, CH_3 , or C_2H_3 fragments from self-assembled monolayers [13]. Despite these pioneering studies, many mechanistic questions about atom abstraction remain unaddressed: What is the nature of the transition state? Is the abstracted fragment transferred as a neutral or charged moiety? How is energy consumed or partitioned in the reaction?

The strong binding energy of oxygen on aluminum makes O-atom abstraction difficult in the present system. It is commonly accepted that oxygen adsorption on Al(111) is characterized by two adsorption phases: chemisorption and oxide formation [14,15]. When O_2 dissociatively chemisorbs on initially clean Al(111), the surface becomes dressed with individual O atoms and (1×1) islands of O atoms, as revealed by scanning tunneling microscopy [15]. Although the coverage of isolated chemisorbed atoms does not grow above 0.04 monolayers (ML), the amount of oxygen atoms located within the islands continues to increase with the overall surface coverage [15]. Oxide growth commences when the oxygen exposure reaches 60 L ($1 \text{ L} = 10^{-6} \text{ torr} \cdot \text{s}$), the equivalent of 0.13 ML. Further oxygen uptake leads to a coexistence of the chemisorbed and oxide phases.

To explore the dynamics of atom abstraction, state-selected $\text{NO}^+(X^1\Sigma^+)$ is scattered on O/Al(111), and NO_2^- is detected. Details of the experimental configuration are described elsewhere [16]. Briefly, scattering takes place in an ultrahigh vacuum chamber consisting of a pulsed molecular beam, a laser ionization source, electrostatic optics for ion transport, a quadrupole mass spectrometer (QMS), an ion sputtering gun for surface cleaning, Auger electron spectroscopy (AES), and low-energy electron diffraction (LEED) for surface characterization, and an ion imaging detector.

The incident NO^+ ions are created in a state-specific manner at the intersection of a supersonic, nitric oxide

beam and the frequency-doubled output of a Nd:YAG-pumped dye laser. $2 + 1$ resonance enhanced multiphoton ionization through the $H/\Pi(\nu = 0)$ Rydberg state produces ions in the ground electronic state, $\text{NO}^+(X^1\Sigma^+)$, in predominantly the $\nu = 0$ vibrational level [17]. The state-selected ions are extracted, accelerated, mass selected, and finally decelerated to 5–80 eV before impinging on a clean or oxygen-covered Al(111) surface. The pulsed ion beam typically delivers $\sim 4 \times 10^4$ NO^+ ions per laser shot, corresponding to an exposure rate of 10^{-5} L per h. Thus, it is reasonable to assume that the surface coverage is not significantly modified by the impinging NO^+ ions during the experiment. The chamber pressure stays below 2×10^{-10} torr when the ion source is running. Surface cleaning comprises several cycles of Ar^+ sputtering (1000 eV, $6 \mu\text{A}$ ion beam directed 60° from the surface normal; $T_s = 300$ K) followed by annealing to 775 K. The cleaning cycles are repeated until contaminant peaks (mainly oxygen and carbon) are absent from the AES spectra, and the LEED pattern shows sharp spots with a low background. Before introducing the NO^+ beam, the surface is dosed with high-purity molecular oxygen through a leak valve. During the dose, the H_2O partial pressure remains less than 1% of the oxygen partial pressure as determined by QMS measurements. Typical doses require 1×10^{-7} torr O_2 for periods up to 40 min. The surface temperature is fixed at 300 K through both the dosing and scattering phases of the experiment.

The incident and scattered ions are monitored with an ion-imaging detector specifically designed to afford mass-to-charge-, angle-, and velocity-resolution with near single-ion detection efficiency [18]. The mass resolution of this detector is achieved by pulsed extraction of the ions into a field-free flight tube where they disperse according to their drift velocity. The extracted ions are intensified by a pair of channel electron multiplier array (CEMA) plates before being imaged on a phosphor screen. By gating the CEMA plates, only ions with a specific mass-to-charge ratio are imaged. The image is captured by a charge-coupled device (CCD) camera and digitized on a computer for storage and processing. The spatial distribution of ions recorded within a given CCD image reflects the ions' two-dimensional velocity distribution in the scattering plane. The detector has acceptance angles of $\pm 28^\circ$ (in-plane) and $\pm 7^\circ$ (out-of-plane). The imaging detector is positioned along the ion-beam axis, which is collinear with the surface normal. This normal-incidence/normal-detection scattering geometry enables the imaging detector to collect incident NO^+ ions and scattered products on alternating laser shots. In this way, a relative ion yield is calculated from the number of collected product ions, integrated over all velocities within the angular range of the detector, and divided by the number of incident ions. An experiment involves monitoring the relative yield, at a desired product mass, as a function of the NO^+ collision energy and the oxygen dose applied to Al(111) prior to scattering. Background levels were determined

by collecting product ions with the surface moved out of the way or by scattering from a clean surface. In both cases, less than one false ion count was registered for every 5×10^8 NO^+ ions incident on the surface. NO^+ , NO^- , NO_2^- , and O^- are all observed in the experiment. Detection of NO_2^- represents the first evidence that incident molecular ions can directly abstract oxygen atoms from a surface; hence, this Letter focuses exclusively on the mechanism responsible for NO_2^- production.

Figure 1 shows the dependence of the NO_2^- yield on oxygen exposure for NO^+ incident with 40 eV collision energy. At zero oxygen exposure, the NO_2^- yield vanishes within the error bars. A linear increase is observed for doses ranging from 0–500 L, followed by a more gradual increase for doses up to 1000 L. Because the NO_2^- yield scales with the total coverage of oxygen rather than the coverage of any particular oxygen species on the surface, the abstraction probability appears to be relatively insensitive to the oxygen chemisorption site.

The survival probability of NO^+ incident on O/Al(111) at 40 eV collision energy is approximately 10^{-7} . Such a low measured value indicates that NO^+ is efficiently neutralized on the inbound trajectory prior to surface impact. Only the ground electronic state $\text{NO}(X^2\Pi)$ can be filled by resonant electron capture from the valence band of aluminum or its oxide. Although electron attachment to form $\text{NO}^-(X^3\Sigma^-)$ can occur close to the surface, its efficiency should be low, because the electron affinity of NO (0.026 eV) is small compared with the work function (≥ 4.3 eV). This argument is confirmed by the low yield ($< 10^{-7}$) of scattered NO^- in this system. Consequently, most of the projectiles impacting the surface are expected to be neutral $\text{NO}(X^2\Pi)$.

Figure 2 presents the NO_2^- yield as a function of $\text{NO}^+(X^1\Sigma^+)$ collision energy for a surface dosed with 750 L O_2 . The NO_2^- yield exhibits a threshold energy of 9 ± 1 eV, above which the yield increases linearly

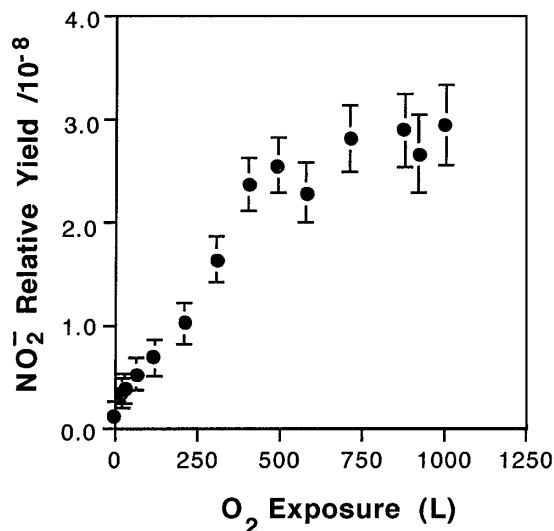


FIG. 1. Relative yield of scattered NO_2^- as a function of oxygen exposure for NO^+ incident at 40 eV collision energy.

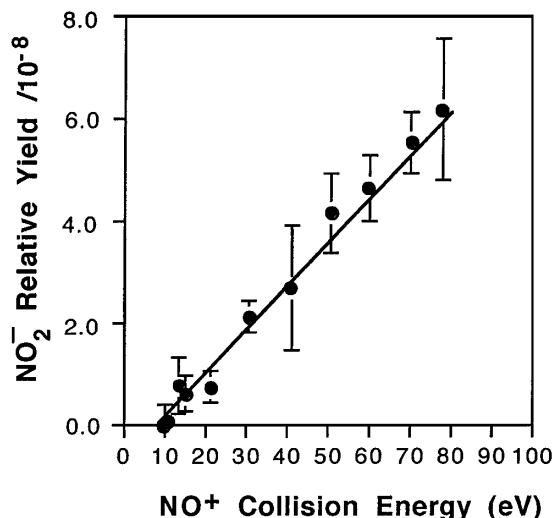


FIG. 2. The collision-energy dependence to NO_2^- emergence. The Al(111) surface was dosed with 750 L O_2 prior to NO^+ scattering. The straight line is drawn to guide the eye.

with NO^+ translational energy. Potential mechanisms for NO_2^- formation include (i) sputtering, (ii) collision-induced recombination, (iii) collision-induced desorption followed by gas-phase association, and atom abstraction by either a (iv) Langmuir-Hinshelwood or (v) Eley-Rideal mechanism. The following discussion will address the feasibility of each mechanism. (i) Sputtering of NO_2 contaminants on the surface is unlikely, because NO_2 dissociates completely on Al(111) and does not adsorb on Al_2O_3 at room temperature [19,20]. (ii) The collisional deposition of energy by an incident projectile may, in principle, induce the recombinative desorption of two or more adsorbates. However, NO and O_2 do not exist as molecular adsorbates on the surface [20,21], and the three-atom recombination involving one adsorbed nitrogen and two adsorbed oxygen atoms is energetically and sterically implausible. (iii) Kang attributed the formation of a scattered complex, CsX^+ , where Cs^+ is the incident projectile and X is an adsorbate, to a two-step mechanism: collision-induced desorption of X followed by gas-phase association in which Cs^+ and X are united by ion-dipole interactions [22]. If this were the operative mechanism in the present study, i.e., the ejected NO-O^- molecule is formed by gas-phase association of scattered NO and sputtered O^- , then the threshold for NO_2^- emergence would be greater than or equal to the threshold for sputtered O^- . Anion emission experiments for Na^+ incident on O/Al reveal a 50 eV threshold for O^- sputtering [23]. This is much higher than the 9 eV threshold observed for NO_2^- emergence; therefore, the ion-dipole association mechanism cannot be operative. (iv) The abstraction of an adsorbed O atom by incident NO can occur by either LH or ER mechanisms. In an LH mechanism, the incident NO would thermally accommodate on the surface, diffuse to a chemisorbed oxygen site, react, and desorb as NO_2 . However, the velocity distribution of scattered NO_2^-

products is nonthermal and cannot be described by a Maxwell-Boltzmann distribution at the surface temperature (300 K). Moreover, the mean translational energy of scattered NO_2^- increases with NO^+ collision energy (see Fig. 3). The data indicate that neither the incident NO molecule nor the scattered NO_2^- product resides on the surface long enough to become thermally accommodated. (v) Instead, it is proposed that NO_2^- is formed by a three-step mechanism: incident NO^+ is neutralized close to the surface, nascent NO directly impacts an adsorbed oxygen atom, and O^- is abstracted by NO to form NO_2^- via an ER mechanism. Within the ER mechanism, the NO_2^- product retains “memory” of the incident NO^+ velocity.

The energetics of the proposed Eley-Rideal mechanism are estimated from published thermodynamic data. Neutralization of incident NO^+ creates vibrationally excited $\text{NO}(X^2\Pi)$ and a hole in the valence band that rapidly delocalizes. Estimates of the Franck-Condon overlap between $\text{NO}^+(X^1\Sigma^+)$ and $\text{NO}(X^2\Pi)$ suggest that 0–2 eV of vibrational energy may be deposited into the nascent NO molecule. *Ab initio* calculations modeling 0.25 ML of oxygen on Al(111) predict that each chemisorbed O atom is bound to the surface by 7.9 eV [24,25]. Theory indicates that oxygen resides on the surface with a -1 rather than a -2 charge, because the adsorbed O atom is not completely coordinated with aluminum ions, as it is in bulk Al_2O_3 . The energy required to remove a chemisorbed O atom from Al(111) and generate an O^- ion in the vacuum is 10.7 eV. The dissociation energy corresponding to $\text{NO}_2^- \rightarrow \text{NO} + \text{O}^-$ is 3.9 eV, as calculated from the 3.1 eV [26] dissociation energy of NO_2 and the electron affinities of O (1.46 eV) and NO_2 (2.27 eV). Consequently, the observed reaction, $\text{NO} + \text{O}^-/\text{Al} \rightarrow \text{NO}_2^- + \text{Al}$ is endoergic by

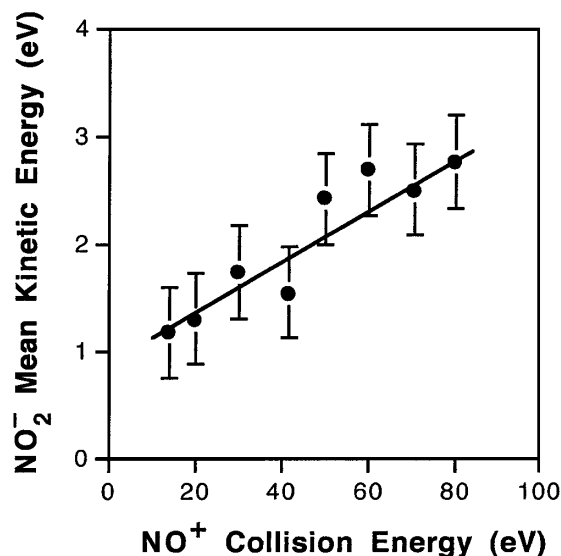


FIG. 3. Mean translational energy of scattered NO_2^- versus collision energy of incident NO^+ . The Al(111) surface was dosed with 750 L O_2 . The straight line guides the eye.

6.8 eV, if neutralization of NO^+ exclusively populates $\text{NO}(X^2\Pi, \nu = 0)$. To the extent that NO is vibrationally excited after NO^+ is neutralized, the energetic requirements for NO_2^- production will be reduced to ~ 4.8 eV.

At threshold, the collision energy (9 eV) minus the sum of the reaction endoergicity and the product kinetic energy (1.1 eV from Fig. 3), represents the energy (1–3 eV) dissipated by the surface and/or deposited as internal energy into NO_2^- . Although depositing 10%–30% of the incident energy into lattice vibrations seems small, it should be noted that at the reaction threshold, only a limited set of trajectories successfully lead to reaction. Successful trajectories necessarily involve impact parameters and bond orientations ideal for efficient activation of the reaction and correspondingly inefficient energy dissipation to the surface. At higher collision energies, trajectories with varying energy deposition will contribute to the reaction probability. The slope of the line drawn in Fig. 3 indicates that $(2.3 \pm 1.0)\%$ of the NO^+ collision energy appears as translational energy in the NO_2^- product. NO_2^- emergence involves the deceleration of the scattered anion as it escapes from the attractive electrostatic potential of the surface. A prior study on a similar system (NO^+ on GaAs) showed that the charge transfer product NO^- scatters with only 6% of the NO^+ collision energy. With the masses of aluminum and oxygen being less than those of gallium and arsenic, and with the mass of NO_2 being greater than that of NO, kinematic arguments correctly predict that the present system should exhibit a greater degree of mechanical energy transfer to the surface than that seen for $\text{NO}^+/\text{GaAs}(110)$.

The abstraction of an O atom from O/Al(111) is expected to have a low probability, because the reaction with NO is endoergic by 6.8 eV. However, the recorded relative yield of NO_2^- may be low for the following reasons. The ion imaging detector measures only the fraction of product ions that scatter into the detector's solid angle of collection. It is estimated that less than 10% of the NO_2^- ions emerging from the surface are directed into the detector's active area. Furthermore, various molecular processes may reduce the amount of detected signal. NO_2^- may transfer an electron into the substrate's conduction band before the molecule escapes into the vacuum. Additionally, during the 5–15 μs flight time from the surface to the detector, NO_2^- may undergo autodetachment or unimolecular dissociation if its internal energy exceeds 2.27 or 3.92 eV, respectively [27,28]. Consequently, the reported NO_2^- relative yield underestimates the probability of NO_2^- formation at the surface.

This Letter represents the first report of hyperthermal energy, molecular ions abstracting adsorbed oxygen atoms. The velocity distribution of scattered NO_2^- products provides clear evidence for a direct, Eley-Rideal reaction. Nitric oxide abstracts O atoms predominantly from islands of chemisorbed oxygen/oxide species. The observed 9 eV threshold is consistent with thermodynamic estimates of the reaction energetics.

Support from the National Science Foundation (CHE96-15878) and the Air Force Office of Scientific Research (F49620-98-1-0029) is gratefully acknowledged.

*Present address: Department of Chemistry and Physics, St. Mary's College, Notre Dame, IN 46556.

- [1] C. R. Arumainayagam and R. J. Madix, *Prog. Surf. Sci.* **38**, 1 (1991).
- [2] D. C. Jacobs, *J. Phys. C* **7**, 1023 (1995).
- [3] E. Murad, *Annu. Rev. Phys. Chem.* **49**, 73 (1998).
- [4] W. H. Weinberg, in *Dynamics of Gas-Surface Interactions*, edited by C. T. Rettner and M. N. R. Ashfold (Royal Society of Chemistry, London, 1991), p. 171.
- [5] J. C. Tully, *J. Chem. Phys.* **73**, 6333 (1980).
- [6] E. W. Kuipers, A. Vardi, A. Danon, and A. Amirav, *Phys. Rev. Lett.* **66**, 116 (1991).
- [7] S. A. Buntin, *J. Chem. Phys.* **108**, 1601 (1998).
- [8] C. T. Rettner, *Phys. Rev. Lett.* **69**, 383 (1992).
- [9] C. T. Rettner, *J. Chem. Phys.* **101**, 1529 (1994).
- [10] C. T. Rettner, D. J. Auerbach, and J. Lee, *J. Chem. Phys.* **105**, 10 115 (1996).
- [11] C. T. Rettner and D. J. Auerbach, *Phys. Rev. Lett.* **74**, 4551 (1995).
- [12] W. Qinyuan and L. Hanley, *J. Phys. Chem.* **97**, 2677 (1993).
- [13] M. R. Morris, D. E. Riederer, Jr., B. E. Winger, R. G. Cooks, T. Ast, and C. E. D. Chidsey, *Int. J. Mass Spectrom. Ion Process.* **122**, 181 (1992).
- [14] I. P. Batra and L. Kleinman, *J. Electron. Spectrosc. Relat. Phenom.* **33**, 175 (1984).
- [15] H. Brune, J. Winterlin, J. Trost, G. Ertl, J. Wiechers, and R. J. Behm, *J. Chem. Phys.* **99**, 2128 (1993).
- [16] J. S. Martin, J. N. Greeley, J. R. Morris, B. T. Feranchak, and D. C. Jacobs, *J. Chem. Phys.* **100**, 6791 (1994).
- [17] Franck-Condon overlap between the $H^1\Pi(\nu = 0)$ Rydberg state and the $X^1\Sigma^+$ ion state predicts a strong propensity for $\Delta\nu = 0$ transitions in the ionization step. Furthermore, there is no evidence for autoionization or strong mixing within the ionization continuum at these photon energies.
- [18] D. Corr and D. C. Jacobs, *Rev. Sci. Instrum.* **63**, 1969 (1992).
- [19] H. Schlienz, M. Beckendorf, U. J. Katter, T. Risse, and H. J. Freund, *Phys. Rev. Lett.* **74**, 761 (1995).
- [20] T. J. Chuang, R. Schwarzwald, and A. Mödl, *J. Vac. Sci. Technol. A* **9**, 1719 (1991).
- [21] A. Hoffman, T. Maniv, and M. Folman, *Surf. Sci.* **183**, 484 (1987).
- [22] M. C. Yang, C. H. Hwang, and H. Kang, *J. Chem. Phys.* **107**, 2611 (1997).
- [23] J. C. Tucek and R. L. Champion, *Surf. Sci.* **382**, 137 (1997).
- [24] G. Wahnstrom, A. B. Lee, and J. Stromquist, *J. Chem. Phys.* **105**, 326 (1996).
- [25] J. Jacobsen, B. Hammer, K. W. Jacobsen, and J. K. Norskov, *Phys. Rev. B* **52**, 14 954 (1995).
- [26] R. Jost, J. Nygard, A. Pasinski, and A. Delon, *J. Chem. Phys.* **105**, 1287 (1996).
- [27] B. A. Huber, P. C. Cosby, J. R. Peterson, and J. T. Moseley, *J. Chem. Phys.* **66**, 4520 (1977).
- [28] E. Anderson and J. Simons, *J. Chem. Phys.* **66**, 2427 (1977).